ChemPubSoc Europe

DOI: 10.1002/cssc.201700297

CHEMSUSCHEM Full Papers

Bifunctional Molybdenum Polyoxometalates for the Combined Hydrodeoxygenation and Alkylation of Lignin-Derived Model Phenolics

Eric Anderson[+], Anthony Crisci[+], Karthick Murugappan, and Yuriy Román-Leshkov*[a]

Reductive catalytic fractionation of biomass has recently emerged as a powerful lignin extraction and depolymerization method to produce monomeric aromatic oxygenates in high yields. Here, bifunctional molybdenum-based polyoxometalates supported on titania (POM/TiO_2) are shown to promote tandem hydrodeoxygenation (HDO) and alkylation reactions, converting lignin-derived oxygenated aromatics into alkylated benzenes and alkylated phenols in high yields. In particular, anisole and 4-propylguaiacol were used as model compounds for this gas-phase study using a packed-bed flow reactor. For anisole, 30% selectivity for alkylated aromatic compounds (54% C-alkylation of the methoxy groups by methyl balance) with an overall 72% selectivity for HDO at 82% anisole conversion was observed over $H_3PMo_{12}O_{40}/TiO_2$ at 7 h on stream. Under similar conditions, 4-propylguaiacol was mainly converted into 4-propylphenol and alkylated 4-propylphenols with a selectivity to alkylated 4-propylphenols of 42% (77% C-alkylation) with a total HDO selectivity to 4-propylbenzene and alkylated 4-propylbenzenes of 4% at 92% conversion (7 h on stream). Higher catalyst loadings pushed the 4-propylguaiacol conversion to 100% and resulted in a higher selectivity to propylbenzene of 41%, alkylated aromatics of 21% and alkylated phenols of 17% (51% C-alkylation). The reactivity studies coupled with catalyst characterization revealed that Lewis acid sites act synergistically with neighboring Brønsted acid sites to simultaneously promote alkylation and hydrodeoxygenation activity. A reaction mechanism is proposed involving activation of the ether bond on a Lewis acid site, followed by methyl transfer and C-alkylation. Mo-based POMs represent a versatile catalytic platform to simultaneously upgrade lignin-derived oxygenated aromatics into alkylated arenes.

Introduction

Lignocellulosic biomass, composed primarily of cellulose, hemicellulose, and lignin, has widely been touted as a source for renewable chemicals and fuels.[1–3] Hemicellulose and cellulose are both polysaccharides, whereas lignin is an aromatic polymer built by oxygenated aromatic monomers linked with a variety of C–O and C–C bonds.[4,5] Although lignin could theoretically generate valuable aromatic chemicals and fuel additives, technical challenges around its selective depolymerization and upgrading have prevented its widespread use as a renewable feedstock.

Currently, biorefineries target optimal sugar utilization to maximize bioethanol production. The first step in lignocellulosic biomass processing involves removing lignin by chemical processes.[6–8] These pretreatments significantly alter the chemical structure of native lignin and generate large streams of technical lignin that is burned for process heating. Technical lignin is burned because it contains highly recalcitrant C–C linkages that render the material unsuitable for selective depolymerization to monomers.[9,10]

Recently, reductive catalytic fractionation (RCF) has emerged as a promising method to extract and selectively depolymerize lignin into monomers and dimers from raw biomass feedstock.[11–16] RCF is typically performed in the presence of protic solvents at temperatures ranging from 453–523 K using supported transition metal catalysts (e.g., ruthenium, palladium, or nickel) and hydrogen gas or other hydrogen transfer agents (e.g., methanol, isopropyl alcohol, or formic acid) as reductants.[17–19] The RCF process generates two highly valuable streams: a carbohydrate-rich solid residue (>90% carbohydrate retention) and a lignin-rich bio-oil (>70% lignin extraction) that contains high concentrations of monomeric aromatic species. Notably, the RCF of hardwoods (e.g., birch and poplar) have been shown to generate total yields of 4-propylguaiacol and 4-propylsyringol as high as 40–50 C mol%.[11,20]

Unfortunately, these lignin-derived monomers cannot be directly used as aromatic fuels (diesel additive) and fuel additives owing to their low volatility caused by the high oxygen content (20–25 wt%), which results in high boiling points (>541 K).[21,22] The energy density and volatility of 4-propylguaiacol and 4-propylsyringol can be improved by deoxygenation. In particular, hydrodeoxygenation (HDO) was proven to be an effective reductive method for cleaving aromatic C–O bonds by hydrogenolysis. Many different materials have been

[a] E. Anderson,[+] Dr. A. Crisci,[+] K. Murugappan, Prof. Y. Román-Leshkov
Department of Chemical Engineering
Massachusetts Institute of Technology
Cambridge, MA (USA)
E-mail: yroman@mit.edu

[+] These authors contributed equally to this work.

Supporting Information and the ORCID identification number(s) for the author(s) of this article can be found under https://doi.org/10.1002/cssc.201700297.

© 2017 Wiley-VCH Verlag GmbH & Co. KGaA, Weinheim

studied for the HDO of aromatic compounds, such as late transition group metals, metal oxides, and metal carbides/phosphides.

Supported late transition metal catalysts have been extensively investigated for the HDO of phenolic model compounds, including eugenol, guaiacol, and phenol.[23–30] Typically, these studies are performed in batch reactions with high hydrogen pressures (3–10 MPa) and temperatures (423–573 K) with reaction times ranging from 1–8 h. Under these conditions, the oxygenated aromatic compounds are saturated to cyclohexanols and then deoxygenated either by HDO or through an acid-catalyzed dehydration to yield alkanes. Recently, Wang et al. also performed HDO on lignin oil produced through the reductive fractionation of poplar wood.[31] In this study, nitrogen-doped ordered mesoporous carbon-supported PtCo nanoparticles converted lignin oil into numerous different alkanes at 10 MPa of H_2 (at temperature), 573 K, and a reaction time of 12 h. Therefore, many materials exhibit high activity for C–O bond hydrogenation, but show poor selectivity for C–O bond cleavage in the presence of C–C double bonds and aromatic bonds. Furthermore, very few materials are capable of directly activating and deoxygenating the aromatic C–O bond of phenolic compounds.

Ideally, the HDO of lignin-derived compounds would yield alkylated aromatics and therefore preserve one of the cardinal features of lignin as well as reducing hydrogen consumption. Typically, when HDO is performed on 4-propylguaicol and 4-propylsyringol, the carbon contained in the methoxy groups of these compounds will be lost as methane. Directly alkylating this carbon onto the aromatic ring simultaneously while removing oxygen will effectively increase both the energy density and the atom economy of the reactions by producing alkylated aromatics while reducing methane production (illustrated in Scheme 1 with anisole as a model compound).

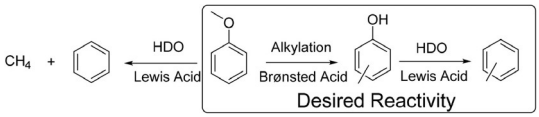

Scheme 1. Possible reaction pathways for anisole conversion.

Performing coupled HDO/alkylation reactions requires bifunctional catalysts that contain both redox and Brønsted acid sites. For example, CoMo sulfide supported on γ-alumina has been used to catalyze coupled HDO/alkylation of anisole at 573 K.[32,33] Although this catalyst has an alkylation selectivity of 28%, it shows a low HDO selectivity of 30% that results in alkyl phenols as the primary products. In contrast, 0.2 wt% Pt on an acidic Beta zeolite converted anisole into alkylated aromatics at 673 K with a selectivity of approximately 50%.[34] Unfortunately, the catalyst lost 50% of its activity by 4 h on stream. Higher Pt loadings resulted in less deactivation.[35] Alkylated phenols can also be produced with bare zeolites.[36,37] Molybdenum carbide—a material featuring redox sites and tunable Brønsted acidity[38–40]—has been shown to be a highly active HDO catalyst, but with low selectivity for alkylation (<1%),[41,42] whereas nickel phosphides have shown improved selectivity for alkylation approaching 15%.[43] We recently demonstrated that molybdenum oxide is highly active for HDO and alkylation, but suffers from over-reduction, phase changes, and eventual deactivation on stream at temperatures above 623 K.[44,45] Further studies showed that the stability of the catalyst improved when the active molybdenum oxide was supported on TiO_2 or ZrO_2.[46] Ceria–zirconia catalysts also show high activity for the demethoxylation of guaiacol to phenol 80–90% with moderate yields of cresols 6–10%.[47]

One alternative to molybdenum oxide for HDO/alkylation reactions are molybdenum-based polyoxometalates (POMs), which have similar redox properties to the oxide, but also contain strong Brønsted acid sites. Keggin-type POMs have the common structure in which twelve metal-oxide clusters consisting of Mo or W surround a central heteroatom such as P or Si. The identity of the central atoms defines the valence of the POM.[48–52] Metal substitutions (e.g, V or Nb) can be made into the external oxide to alter the chemical composition and, consequently, the strength and number of Brønsted acid sites, the redox properties, and the thermal stability of the POM.[48] This tunability was exploited for W- and Mo-based POMs to alter the deoxygenation rates of ketone and carboxylate functional groups by substituting different metals into the external oxide shell.[53–55] POMs offer a highly customizable scaffolding to construct the specific active sites to modulate the dual active site motifs required to promote tandem HDO and alkylation reactions; yet, these materials, have seldom been studied in the context of biomass upgrading.

Herein, we demonstrate that Mo-based Keggin POMs with the formula $H_3PMo_{12}O_{40}$ supported on titania (POM/TiO_2) are effective catalysts to upgrade lignin-derived compounds by coupled HDO/alkylation reactions. The conversion of anisole to alkylated aromatics was investigated to understand the origins of HDO and alkylation reactivity, as well as the resulting product distribution. In addition, 4-propylguaiacol, a direct product from the RCF of lignin, was also deoxygenated to alkylated phenols. Reactivity studies using ethylphenol and ethylbenzene cofeeds with anisole were combined with X-ray photoelectron and infrared spectroscopy to discriminate the types of catalytic sites responsible for reactivity and to propose a plausible mechanism.

Results and Discussion

The reaction profile of anisole over the bifunctional POM/TiO_2 catalyst is shown in Figure 1a. Four types of products are generated based on the combination of HDO and alkylation reactions with the following distribution in C mole%: 44% benzene, 12% alkylated aromatics, 12% alkylated oxygenates, and 4% methane (shown in Figure 1b). Additionally, very little aromatic hydrogenation was observed with the only detectable product being cyclohexene at 0.16 C mol%. This product distribution was observed at 7 h on stream and an anisole conversion of 82%. The selectivity for HDO and alkylation products was 72 and 30%, respectively. The alkylated aromatics ranged

© 2017 Wiley-VCH Verlag GmbH & Co. KGaA, Weinheim

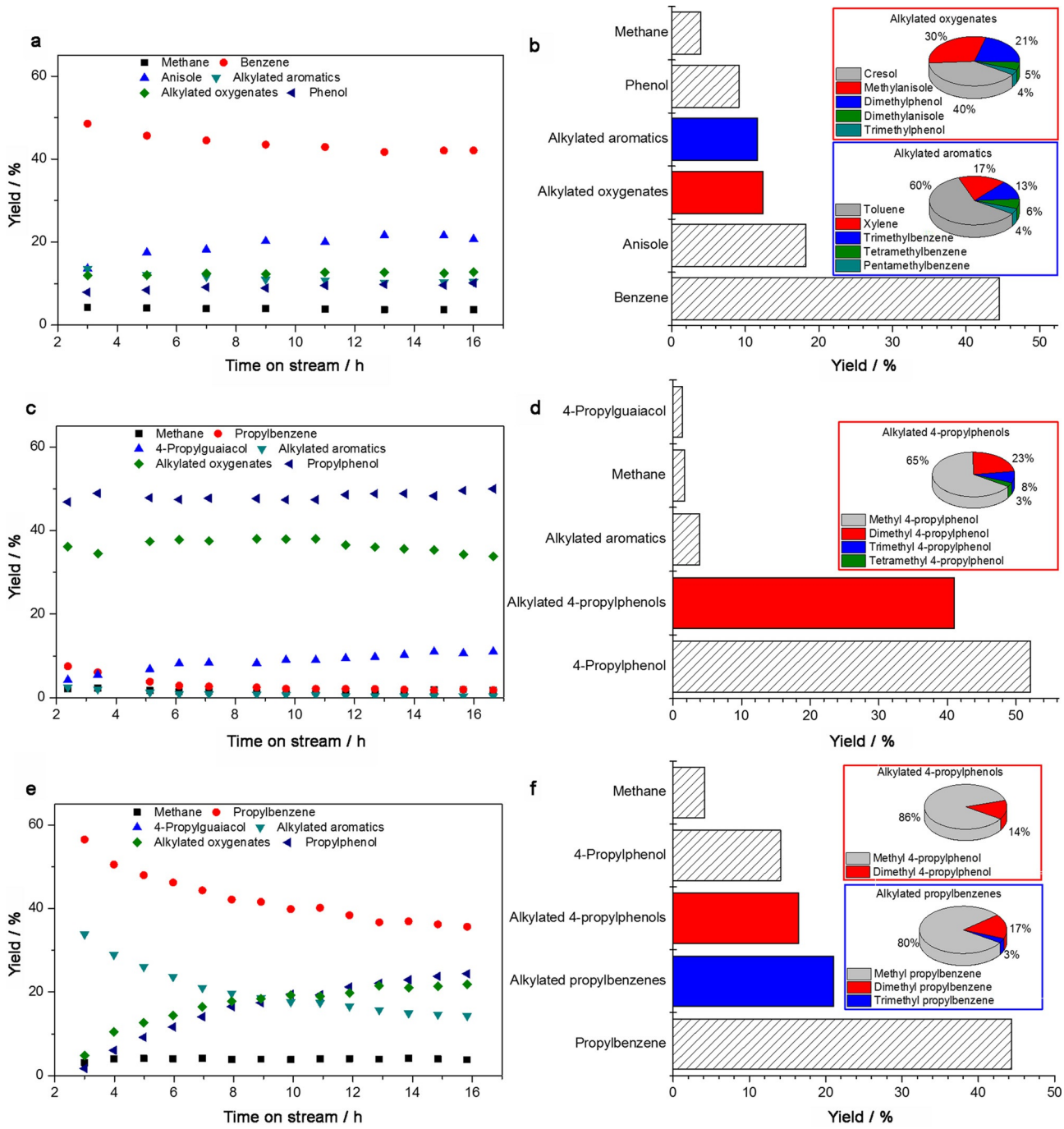

Figure 1. a) Yield (C mole %) for the reaction of anisole (200 μL h^{-1}) over 300 mg of 10% POM/TiO_2 at 593 K, 0.1 MPa (70 mL min^{-1}) H_2 as a function of time on stream. b) Product distribution of binned species at 7 h on stream for the reaction of anisole over POM/TiO_2. c) Yield (C mole %) for the reaction of 4-propylguaiacol over 100 mg of 10% POM/TiO_2 at 593 K, 0.1 MPa (17.5 mL min^{-1} H_2 and 52.5 mL min^{-1} N_2) as a function of time on stream. d) Product distribution of binned species at 7 h on stream during the reaction of 4-propylguaiacol over 100 mg of POM/TiO_2. e) Yield (C mole %) for the reaction of 4-propylguaiacol over 300 mg of 10% POM/TiO_2 at 593 K, 0.1 MPa (17.5 mL min^{-1} H_2 and 52.5 mL min^{-1} N_2) as a function of time on stream. f) Product distribution of binned species at 7 h on stream during the reaction of 4-propylguaiacol over 300 mg of POM/TiO_2. 4-propylguaiacol was fed as a 5 wt% solution in toluene at 900 μL h^{-1}.

from toluene up to pentamethylbenzene with the yield of each alkylated product being inversely proportional to the number of methyl groups on the aromatic ring. The yield of alkylated oxygenates mirrors the product distribution of the alkylated aromatics, as observed in the inset of Figure 1 b. The alkylated oxygenates can exist as either phenolic alkylated oxygenates (e.g., cresol) or as alkylated phenolic ethers (e.g., methylanisole). The total alkylated oxygenates comprised mainly phenolic compounds (ca. 70%). A mole balance on the methyl groups was used to track the amount of alkylation, given that a calculation based on C mole% does not allow the quantitation of the actual degree of alkylation. The mole

© 2017 Wiley-VCH Verlag GmbH & Co. KGaA, Weinheim

balance of the anisole-derived methyl groups shows that 54% of the methyl groups were alkylated onto the aromatic ring and the remaining 46% was converted to methane.

The reactivity profile for anisole conversion presented in Figure 1a shows that a 3 h transient period is needed to achieve steady-state and that the catalyst loses only 5% of this activity after 16 h on stream. We note that the alkylation selectivity was relatively constant throughout the reaction and that the decrease in anisole conversion was solely owed to a decrease in HDO activity, as evidenced by the corresponding decrease in benzene yield. The mass balance based on condensable liquids and methane over a 16 h reaction was 86% given that some of the more volatile products escaped the condenser over the 16 h experiment.

For 4-propylguaiacol, when an experiment was performed with 100 mg of 10% POM/TiO_2 (0.26 h mass-averaged contact time), the conversion remained above 90% over the course of the 16 h experiment (shown in Figure 1c). Specifically, at 7 h on stream, the 4-propylguaiacol conversion was 92% with an alkylation selectivity of 42%. The mole balance around the methoxy group of 4-propylguaiacol showed that 77% of methyl groups were alkylated onto the aromatic rings. The HDO selectivity of 4-propylguaiacol to fully deoxygenated products was only 4%, but the HDO selectivity to 4-propylphenols and alkylated 4-propylphenols was 93%. The alkylated products follow the same trend as that observed for anisole (shown in Figure 1d). Additionally, no 4-propylcatechol was observed, indicating that complete deoxygenation of the methoxy group occurred during the reaction. The catalyst clearly promoted deoxygenation of the weaker methoxy group of 4-propylguaiacol as opposed to the stronger phenolic group, as evidenced by the low yield of propylbenzene and alkylated propylbenzenes.

To tailor the product distribution to produce completely deoxygenated products, such as propylbenzene and alkylated propylbenzenes, the experiment with 4-propylguaiacol was repeated with a longer mass-averaged contact time of 0.77 h. Under these conditions, 100% of the 4-propylguaiacol feed was converted mainly into propylbenzene and alkylated propylbenzenes (Figure 1e). Specifically, at 7 h on stream, 40, 21, and 17% yields of propylbenzene, alkylated propylbenzenes, and alkylated 4-propylphenol were obtained, respectively. Taken together, these results translate into a 61% yield of completely deoxygenated products with a 38% yield for alkylation (51% of methyl groups were alkylated by mole balance). These data demonstrate that the catalyst is capable of activating and deoxygenating phenolic functional groups at longer contact times. Interestingly, when the space velocity was decreased, the alkylation selectivity decreased from 42 to 38% and the product distribution of alkylated products was altered (shown in Figure 1f). At high conversions, mono- and di-alkylation was favored, whereas at low HDO conversions, up to tetra-alkylation was observed. These results imply that that the oxygen on the aromatic ring influences alkylation rates and selectivity and are further supported by the slightly lower selectivity for alkylation and higher degree of multi-alkylated products observed for anisole when compared to 4-propylguaiacol at high HDO conversions. We hypothesize that the differences in product distribution and yield are likely owed to the additional hydroxyl group present in 4-propylguaiacol. Finally, the rate of phenolic bond cleavage decreased more rapidly when compared to methoxy group cleavage, suggesting a higher deactivation rate when full HDO is performed. Over 16 h, the yield of propylbenzene decreased from 56 to 36% with a mirrored increase in the yield of 4-propylphenol.

In Scheme 2, we have outlined a reverse Mars–van Krevelen reaction pathway to yield the main components detailed in Figure 1b.[54,56,57] Specifically, a Lewis acidic vacancy is generat-

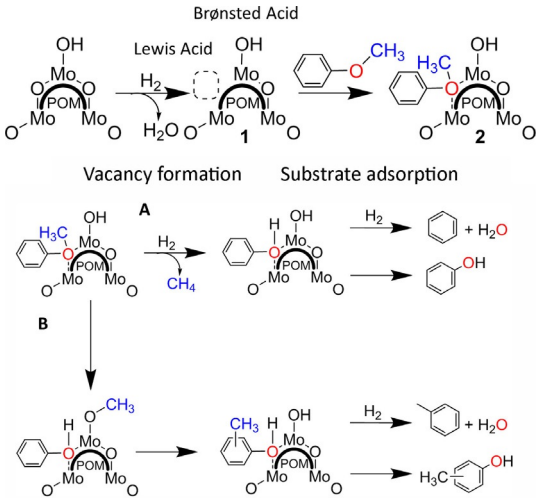

Scheme 2. Proposed reaction network for coupled HDO and alkylation reaction on the surface of POM/TiO_2.

ed by reducing the catalyst surface with H_2.[58] Next, anisole binds onto this oxophilic site through its oxygen atom, giving way to two plausible pathways. In pathway A, the coordinated anisole can undergo hydrogenolysis to produce phenol and methane. The former may either desorb from the catalyst surface or undergo further reduction to form benzene and water. In pathway B, the methyl group of the phenolic ether transfers to an adjacent Brønsted acid site resulting in the production of phenol and an electron-deficient surface bound methyl species. Alternatively, benzene and methanol may be formed through the hydrogenolysis of the aromatic C—O bond. Methanol can form a reactive methoxy species upon interacting with an adjacent Brønsted acid site leading to either intramolecular (to the adjacent adsorbed phenol) or intermolecular (to another adsorbed oxygenated aromatic molecule) C-alkylation. Similarly to pathway A, the oxygenated aromatic substrate can desorb from the catalyst surface leaving a vacancy that can be occupied by another oxygenate susceptible to the same alkylation and deoxygenation, leading ultimately to the production of multi-alkylated aromatics. Regardless of the catalytic pathway followed, the acid sites are always regenerated to close the catalytic cycle.

X-ray photoelectron spectroscopy (XPS) was employed before and after reaction with anisole to investigate the formation of catalytic active sites under reducing conditions. The initial oxidation state of molybdenum in the as-prepared,

© 2017 Wiley-VCH Verlag GmbH & Co. KGaA, Weinheim

unsupported POM is Mo^{VI}. Upon supporting it on TiO_2, some of the molybdenum becomes partially reduced to Mo^{V}. Indeed, TiO_2 is a photosensitive semiconductor that promotes electrons into the conduction band and reduces the POM. The post-reaction sample contains a mixture of Mo^{IV} and Mo^{V} oxidation states after 16 h on stream. This mixed oxidation state is required to form the Lewis acid vacancies in the POM lattice, as illustrated in Figure 2. In addition, a sample that was reduced in H_2 at 593 K for 4 h in the absence of the oxygenate reactant contained a higher proportion of Mo^{IV} than that observed post-reaction after 16 h on stream. We hypothesize that the redox process is altered when an oxidant (oxygenated feed) is present that changes the proportion of Mo^{VI} and Mo^{V} species.

To gain further insight into the nature of the catalytic sites, the acid sites on the material were characterized by ammonia temperature-programmed desorption (TPD) and pyridine adsorption coupled with FTIR. The acid sites of POM/TiO_2 and TiO_2 quantified by NH_3-TPD showed values of 338 and 178 $\mu mol_{NH_3}\, g^{-1}$, respectively (see Table 1). To isolate the role of Lewis acid sites on the reaction network, Brønsted acid protons were exchanged with Na ions to generate a NaPOM material featuring a reduced acid site count of 71 $\mu mol_{NH_3}\, g^{-1}$. FTIR

Table 1. Physicochemical properties of various supported POMs and TiO_2.[a]

Sample	Surface area [$m^2\, g^{-1}$]	NH_3 adsorption [$\mu mol\, g^{-1}$]
POM	6	–
TiO_2	56.3	178
10% POM/TiO_2	48.1	338
10% NaPOM/TiO_2	43.9	71

[a] Surface area was measured by N_2 adsorption and acid sites were quantified with NH_3-TPD.

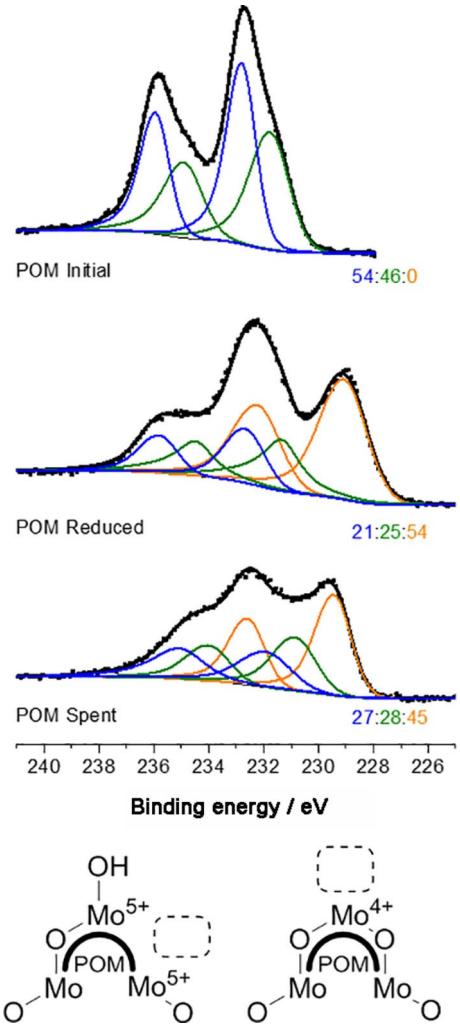

Figure 2. XPS of three supported POMs. POM initial is fresh POM/TiO_2, POM reduced is POM/TiO_2 after 4 hours of reduction at 593 K with H_2, POM spent is POM/TiO_2 after 16 hours of reaction with 200 μL/hr anisole at 593 K in H_2 (70 mL min^{-1}). The numbers in the bottom right denote the distribution of oxidation states from Mo^{VI} to Mo^{IV}. The strucutres located below the XPS data illustrate potential vacancies that could exist in the reduced POM.

spectra of pyridine adsorbed onto unsupported POM showed bands corresponding to Lewis acid sites at 1605 and 1448 cm^{-1} (Figure 3).[59,60] Additional bands were also observed at 1587 and 1487 cm^{-1} corresponding to the oxidative breakdown of pyridine to carboxylate species.[61] Interestingly, no bands associated to pyridine bound to Brønsted acid sites (1636 or 1542 cm^{-1}) were observed.[62,63] The band at 1440 cm^{-1} was associated to hydrogen-bonded pyridine.[61] We hypothesize that this effect is likely owed to solid-state ion exchange with the KBr used to produce the pellets for analysis. Upon reducing the materials under flowing H_2 at 583 K for 2 h, the vibration related to Lewis acidity shifted from 1605 to 1607 cm^{-1} and a new intense, broad band appeared at 1402 cm^{-1}. We attribute this band to the binding of a pyridine molecule between two adjacent Lewis acid sites (designated as the Mo^{V} vacancy in Figure 2), which would result in lower-frequency vibrational modes as a result of the coordination to two metal sites.

Analysis of spent catalysts confirmed that the POM structure exists as a highly reduced phosphomolybdic species. Specifically, the ^{31}P NMR spectra of the unsupported POM showed two

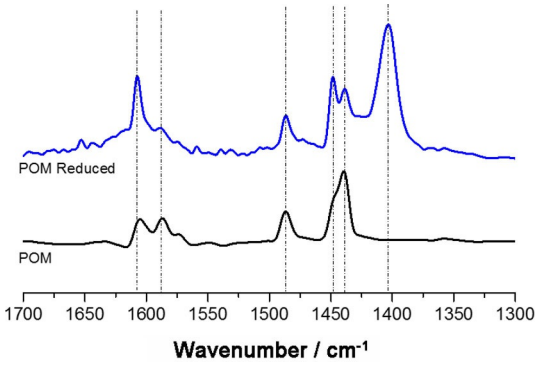

Figure 3. FTIR spectra of pyridine chemisorbed onto unsupported POM and the unsupported POM after reduction. Vertical dashed lines indicate the position of adsorption peaks. In situ reductions were performed at 583 K with pure H_2(20 mL min^{-1}) for 2 h.

© 2017 Wiley-VCH Verlag GmbH & Co. KGaA, Weinheim

distinct chemical shifts observed at −3.2 and −1.6 ppm corresponding to molybdenum Keggin POM and the lacunary POM derivative, respectively.[52,64] Notably, the fresh POM/TiO_2 materials also features these two resonances but also exhibits an additional resonance at −4.8 ppm, which is attributed to the reduced POM state observed by XPS (Figure 4). Both a POM/TiO_2 sample reduced under H_2 and the spent catalyst did not contain the resonances associated with the lacunary and Keggin POM, but instead showed highly shielded phosphorus resonances at −6.8 and −13.2 ppm. The presence of such highly shielded signals implies that a phosphomolybdic polyanion remains intact during the reduction reaction. This phosphomolybdic species was extracted from the catalysts into an aqueous solution and precipitated as a solid. The PXRD pattern for this species is similar to that obtained for the as-synthesized POM (Figure S2), which is strong evidence suggesting that the POM architecture in a reduced state is preserved on the catalyst surface. These results would not have been observed if the POM had decomposed under reaction conditions into water insoluble molybdenum oxide and a surface phosphate species.

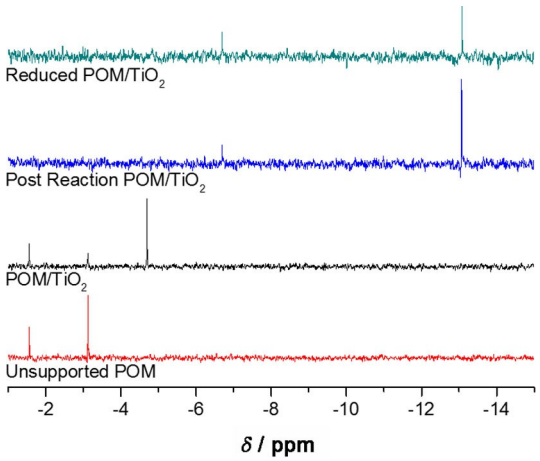

Figure 4. Solution phase ^{31}P NMR of POMs in D_2O. In these samples, the POM catalyst was extracted off of the surface of the support with D_2O acidified with phosphoric acid. Reduced POM is POM/TiO_2 after 4 hours of reduction at 593 K with H_2. Post-reaction POM is POM/TiO_2 after 16 hours of reaction with 200 μL h^{-1} anisole at 593 K in H_2 (70 mL min^{-1}).

Control reactions were performed to gain insight into the reaction mechanism (Figure S3). First, a reaction in the absence of hydrogen over POM/TiO_2 resulted in an anisole conversion of <5%, implying that hydrogen is critical towards generating reaction sites capable of performing HDO/alkylation reactions. The experiment without hydrogen was repeated with a 30 mole% water cofeed yielding a 10% anisole conversion into phenol as the primary product. The low C–O bond cleavage rates imply that acid catalyzed hydrolysis is not responsible for the high anisole conversion observed with hydrogen gas. Note that while the catalyst innately possesses Lewis and Brønsted acid sites, these sites did not result in significant turnovers in the absence of hydrogen. To directly investigate the role of the Brønsted acidity, anisole was also reacted over NaPOM/TiO_2 under regular reaction conditions. The NaPOM/TiO_2 featured an anisole conversion of 18%, and primarily produced benzene. Less than 1 Cmole% of the products were alkylated, thus showing that HDO activity dominates in the absence of Brønsted acidity. Experiments performed with the bare TiO_2 support in flowing hydrogen resulted in anisole conversion values <10%. The reactor effluent contained about 6 Cmole% phenol, 2 Cmole% benzene and alkylated aromatics, and 2 Cmole % of the alkylation product, methylanisole. Although TiO_2 is known to possess both Lewis and Brønsted acid sites, these data show that the support does not promote HDO/alkylation to a significant extent.

It was observed in the 4-propylguaiacol runs that the alkylation rate and the product distribution are impacted by the degree of deoxygenation. To study this effect, anisole was cofed into the reactor with either an equimolar amount of ethylbenzene or ethylphenol while keeping the total molar flow of oxygenates constant (Figure 5). When compared to a pure anisole feed base case, an ethylbenzene cofeed resulted in a decrease in the anisole alkylation selectivity from 54 to 47% at similar conversions of 81 and 96%, respectively. Interestingly, although no ethylbenzene alkylation products (e.g., ethyltoluene) were observed, cofeeding ethylphenol yielded mixed alkylation products, such as methylethylphenol. The addition of ethyl phenol also resulted in a lower conversion of the anisole (75%). Given that mixed alkylation occurs with ethylphenol,

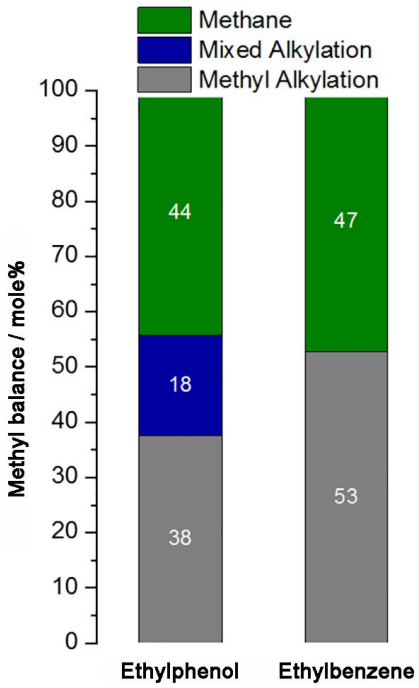

Figure 5. Mole balance performed around the methoxy group of anisole with different cofeeds. The methyl alkylation bin is defined as the mole % of methoxy groups that went into alkylating anisole. The mixed alkylation bin signifies the fraction of methoxy groups that alkylated the cofeed such as methylethylbenzene and methylethylphenol. The experiment with ethyl benzene had 5% unreacted methoxy groups whereas the experiment performed with ethyl phenol had 30% unreacted methoxy species.

© 2017 Wiley-VCH Verlag GmbH & Co. KGaA, Weinheim

but not with ethylbenzene, we hypothesize that the presence of oxygen is essential for the alkylation reaction to occur. This observation is consistent with the 4-propylguaiacol results that resulted in the highest yield of alkylated products when the HDO conversion was the lowest. Furthermore, when the HDO conversion was increased, the reaction favored mono- and di-alkylation products because the oxygen was removed before additional alkylation reactions could occur. We posit that the presence of oxygen in the molecular structure either allows the binding to the surface for the reaction to occur or provides electron density to promote electrophilic aromatic substitution. Additionally, the formation of mixed alkylation products supports the proposed alkylation pathway in Scheme 2, as alkyl groups are leaving the anisole and coupling onto a different oxygenate. Ultimately, the two reactions are highly coupled because the yield of alkylated products is low with no HDO activity, but is also reduced at high HDO conversion.

Conclusions

Molybdenum-based polyoxometalates (POMs) were demonstrated to be highly active bifunctional catalysts for coupled hydrodeoxygenation (HDO) and alkylation of lignin model compounds. Specifically, these catalysts convert anisole into a range of alkylated arenes with alkylation and HDO selectivity values of 30 and 72%, respectively, at 82% conversion after 7 h on stream. 4-Propylguaiacol, a product from the reductive catalytic fractionation (RCF) of lignin, was also deoxygenated over POM/TiO_2. Under the conditions tested, a 4-propylguaiacol conversion of 92% was observed with an alkylation selectivity of 42% to alkylated phenols. A low amount of catalyst deactivation was observed with a drop in reactant conversion of <10% over 16 h for both reactants. Additionally, a high conversion reaction was performed with 4-propylguaiacol resulting in a 40% yield of propylbenzene, 21% yield of alkylated propylbenzenes, and a 17% yield of alkylated 4-propylphenol. Finally, a potential reaction mechanism for HDO and alkylation was postulated. The mechanism is based on catalyst characterization such as X-ray photoelectron spectroscopy (XPS), FTIR pyridine adsorption, and additional reactivity studies with multi-component feeds. Insights into the active sites of the catalyst now allow for further catalyst optimization through metal substitutions to modulate the Brønsted acidity and Lewis acidity of the catalyst. Ultimately, balancing these two functionalities will further improve the HDO/alkylation selectivity of the catalyst.

Experimental Section

Catalyst Synthesis: Molybdenum oxide (99.5%, Sigma–Aldrich) was added to deionized water to a concentration of 0.13 g mL^{-1}. The slurry was added to a 250 mL two-neck, round bottom flask with a magnetic stir bar. The slurry was then heated to 373 K and allowed to reflux. Next, 85 wt% phosphoric acid (2 g, 1.5 equivalents per mole of molybdenum, Sigma–Aldrich) was quickly added to the slurry and the slurry was allowed to reflux for 36 h. The yellow-green solution was then filtered to remove residual molybdenum oxide. The resulting POM was recovered from the aqueous solution by evaporation. Given the low surface area of the POM, it was supported on nanosized titanium oxide (99.5%, Sigma–Aldrich, primarily anatase) by dissolving the solid POM in water and adding the solution dropwise to the support while mixing vigorously. The water was removed by drying in a 393 K oven overnight. The nominal POM/TiO_2 catalyst loading was 10 wt%. The identity of the material was confirmed by ^{31}P nuclear magnetic resonance (NMR), powder X-ray diffraction (PXRD) and IR spectroscopy.[51,65] The sodium form of the POM, denoted NaPOM, was prepared by ion exchange with a Na amberlyst (Sigma Aldrich) resin. The ion exchange was performed by dissolving the POM in DI water and mixing it with an amount of resin equivalent to a fivefold molar excess of Na for 24 hours. This procedure was repeated twice to achieve full Na exchange.

Reactivity Studies: The vapor-phase reactions were performed in a packed-bed reactor. The reactor was constructed from a 0.95 cm outer diameter (OD) (0.089 cm wall thickness) stainless-steel tube with a welded lip in the center. The reactor was mounted inside a single stage furnace (850 W/115 V, Applied Systems Series 3210). The temperature of the bed was controlled by a thermocouple (Omega, model TJ36-CAXL-116u) positioned downstream of the bed and connected to a temperature controller (Digi-sense, model 68900-10). The catalyst bed was supported on a glass wool plug. The bed consisted of two inert segments of α-alumina (100–200 mesh) on the top and bottom of the catalyst bed. The catalyst bed was made by homogenously distributing 300 mg for reactions with anisole or 100 mg for reactions with 4-propylguaiacol of 10% POM/TiO_2 (100–140 mesh) in α-alumina (100–200 mesh) for a total bed weight of 1 g. Anisole was introduced into the reactor through a syringe pump (Harvard Apparatus, model 703005) at a flow rate of 200 $\mu L\,h^{-1}$. These experiments were performed at atmospheric pressure and at a gas flow rate of 70 $mL\,min^{-1}$ (90/1 H_2/anisole molar ratio, equivalent to a mass-based contact time of 0.15 h). Experiments with 4-propylguaiacol were done with toluene as a solvent. Specifically, a solution of 5 wt% 4-propylguaiacol in toluene was fed to the reactor at a flow rate of 900 $\mu L\,h^{-1}$. To account for the reduced 4-propylguaiacol partial pressure, the hydrogen partial pressure was adjusted to maintain a constant H_2/oxygenate molar ratio of 90 (mass-averaged contact time based on total mass loadings of 0.26 h or 0.77 h for long contact time experiments) by flowing 17.5 mL $H_2\,min^{-1}$ (Airgas, 99.999%) with a balance of N_2 (Airgas, 99.999%) with a total gas flowrate of 70 $mL\,min^{-1}$. Reaction conditions were chosen to operate in the absence of mass-transfer limitations.

The reactor effluent was transferred from the reactor to a GC–MS (Agilent 7890 A, Agilent 5975 C) using heated lines at ca. 523 K to avoid condensation. The reaction products were monitored and quantified in real time with a flame ionization detector (GC–FID, Agilent Technologies, model 7890A) and a DB-5 column (Agilent 30 m × 0.25 mm id, 0.25 μm). The conditions used in the analysis were as follows: the gas flow rate was 1.0 $mL\,min^{-1}$ helium (Airgas, 99.999%) or 1.4 $mL\,min^{-1}$ hydrogen in the case of 4-propylguaiacol, the injector temperature was 523 K, the detector temperature was 573 K, and the split ratio was 1:25. The oven temperature ramp started at 308 K and was held for 2 min and was then ramped to 453 K at a rate of 10 $K\,min^{-1}$ for anisole. The final oven temperature was increased to 553 K for the experiment utilizing 4-propylguaiacol. The products were simultaneously identified using a mass-selective detector (MSD, Agilent Technologies, model 5975C). The mass balance was calculated by quantifying both the gas and liquid phase products. Methane was quantified by the

© 2017 Wiley-VCH Verlag GmbH & Co. KGaA, Weinheim

GC–FID and liquid products were condensed in an ethanol bath maintained at 273 K. The liquid phase products were analyzed by GC–FID with an external standard, dodecane. The water in the liquid phase was titrated by Karl–Fischer analysis (Mettler-Toledo, 5131128813).

The following definitions were used to evaluate experimental data and values are based on GC detectable species [Eqs. (1)–(4)]:

$$\text{Conversion} = \frac{\text{reactant consumed [C mol]}}{\text{reactant fed [C mol]}} \quad (1)$$

$$\text{Methyl balance} = \frac{\sum(\text{alkylated products [mol]} \times \text{alkyl groups})}{\sum(\text{alkylated products [mol]} \times \text{alkyl groups}) + CH_4\text{[mol]}} \quad (2)$$

$$\text{Alkylation selectivity} = \frac{\text{alkylated products [C mol]}}{\text{reactant consumed [C mol]}} \quad (3)$$

$$\text{HDO selectivity} = \frac{\text{fully deoxygenated products [C mol]}}{\text{reactant consumed [C mol]}} \quad (4)$$

in which alkylated products refer to any alkylated aromatics or alkylated aromatic oxygenates.

Catalyst Characterization: FTIR spectra were collected with a Bruker Vertex 70 spectrophotometer equipped with an Hg-Cd-Te (MCT) detector. Each spectrum was recorded by averaging 64 scans at 2 cm^{-1} resolution in the 4000–400 cm^{-1} range. Unsupported POM was used for these studies due to the low mass loading and poor compressibility of the titania-supported catalyst. Unsupported POM was pressed into wafers with KBr as a diluent (10% *w/w* POM). The wafers were loaded into a high-temperature transmission cell (Harrick Scientific) with ZnSe windows. The samples were dried at 373 K for 12 hours under vacuum (< 0.01 Pa, dynamic vacuum, Edwards' T-Station 75 Turbopump). After taking a reference spectrum, the sample was dosed with pyridine (Sigma–Aldrich, anhydrous 99.8%) at room temperature, which can adsorb to both Lewis and Brønsted acid sites. The pyridine was dosed by administering pulses of vaporized pyridine at room temperature from a liquid pyridine sample. The pyridine was degassed before adsorption by a freeze-pump-thaw cycle performed at 77 K. The vacuum was then reestablished to remove gas phase and physisorbed pyridine. The resulting vibrational frequencies were used for acid site speciation. A second set of experiments was performed under reducing conditions. Specifically, fresh wafers were prepared and dried as before, and the sample was then reduced with H_2 at 583 K with a gas flow rate of 20 mL min^{-1} for 2 hours. The sample was cooled to room temperature and pyridine dosed onto the sample. The excess pyridine was removed by exposing the sample to vacuum before acquiring a spectrum.

NH_3-TPD was performed using a U-tube reactor setup coupled to a Hiden Analytical HPR20 mass spectrometer. The U-tube reactor consisted of a quartz U-tube mounted in an insulated single-zone furnace (550 W/115 V, Carbolite GTF 11/50/150B). A thermocouple (Omega, model TJ36-CAXL-116u) was mounted within the U-tube slightly above the sample bed, and was connected to a temperature controller (Digi-Sense, model 68900-10). The bed consisted of 300–400 mg (22–38 mesh) of pelletized catalyst. Next, the catalyst was dried under flowing 1% argon in helium (100 mL min^{-1}) at 373 K and then exposed to several pulses of the NH_3, totaling ca. 10 mL at STP. The samples were heated to 823 K (10 K min^{-1}) and held for 30 min at that temperature and the effluent gas containing desorbed ammonia was monitored by mass spectroscopy (tracking the $m/z = 17$ fragment). The MS response was calibrated for each ammonia pulse prior to every analysis.

XPS samples were prepared in a stainless steel U-tube reactor 0.95 cm OD (0.089 cm wall thickness) equipped with two valves located at the inlet and outlet, which allowed the reactor to be sealed. The reactor was heated in an insulated single-zone furnace (550 W/ 115 V, Carbolite GTF 11/50/150B). A thermocouple (Omega, model TJ36-CAXL-116u) was mounted inside the furnace at the same height as the catalyst bed and controlled with a temperature controller (Digi-Sense, model 68900-10). The reaction effluent was monitored by GC–MS. The liquid feed was introduced through a gas saturator located upstream of the reactor. The reactor was packed with 140 mg (100–140 mesh) for these experiments. This was done to maintain a similar anisole conversion to reactivity studies. Once the reaction was completed, the reactor was purged with nitrogen and sealed by the two valves and transferred to a glove box where the XPS samples were prepared. XPS samples were prepared with 10 wt% niobium oxide (99.99%, Sigma–Aldrich) as a standard. The binding energies were corrected to 207.4 eV (Nb $3d_{5/2}$). The samples were transferred to the instrument using a portable transfer vessel, thereby ensuring that samples were not exposed to air. XPS spectra were acquired on a PHI Versaprobe II equipped with a multichannel hemispherical analyzer and aluminum anode X-ray source operating at 100 W with a 100 mm beam scanned over a 1.4 mm line across the sample surface. A dual-beam charge neutralization system was used with an electron neutralizer bias of 1.2 eV and Argon ion beam energy of 10 eV. A 7-point Shirley background correction was then applied to the Mo 3d XPS spectra after charge correction. The composition of Mo oxidation states was estimated by the deconvolution of Mo 3d spectra. The following constraints were used for deconvolution: 1) Splitting energy of 3.15 eV for Mo $3d_{5/2}$–Mo $3d_{3/2}$, 2) area intensity ratio of 3:2 for Mo $3d_{5/2}$–Mo $3d_{3/2}$, and 3) equal full width at half maximum (FWHM) of Mo $3d_{5/2}$ and Mo $3d_{3/2}$.

^{31}P NMR spectroscopy samples were prepared by dissolving the POM in acidified D_2O with phosphoric acid (1.4 mg mL^{-1}, pH 1). The fresh POM, post-reaction POM, and reduced POM were prepared by extracting the POM/TiO_2 with 3–4 mL acidified D_2O for 3 hours. The phosphoric acid used to acidify the D_2O was also used as the NMR reference. A 500 MHz NMR (Bruker) was used to perform the ^{31}P NMR analysis, using a single pulse program with 64 scans. 225 scans were acquired for each sample.

Acknowledgements

We would like to thank the National Science Foundation for supporting the research performed in this work, CBET Award No 1454299.

Keywords: alkylation · biomass · hydrodeoxygenation · molybdenum · polyoxometalates

[1] J. E. Holladay, J. F. White, J. J. Bozell, D. Johnson, *Top Value-Added Chemicals from Biomass, Volume II, Results of Screening for Potential Candidates from Biorefinery Lignin*, DTIC Document, **2007** http://www.pnl.gov/main/publications/external/technical reports/PNNL-16983.pdf.

[2] T. Werpy, G. Petersen, A. Aden, J. Bozell, J. Holladay, J. White, A. Manheim, D. Eliot, L. Lasure, S. Jones, *Top value-added chemicals from biomass. Volume 1, Results of screening for potential candidates from sugars and synthesis gas*, DTIC Document, **2004** http://www.nrel.gov/docs/fy04osti/35523.pdf.

© 2017 Wiley-VCH Verlag GmbH & Co. KGaA, Weinheim

[3] A. J. Ragauskas, G. T. Beckham, M. J. Biddy, R. Chandra, F. Chen, M. F. Davis, B. H. Davison, R. A. Dixon, P. Gilna, M. Keller, P. Langan, A. K. Naskar, J. N. Saddler, T. J. Tschaplinski, G. A. Tuskan, C. E. Wyman, *Science* **2014**, *344*, 1246843.
[4] C. Heitner, D. Dimmel, J. Schmidt, *Lignin and lignans: advances in chemistry*, CRC press, **2016**.
[5] A. Sakakibara, *Wood Sci. Technol.* **1980**, *14*, 89 – 100.
[6] X. Zhao, K. Cheng, D. Liu, *Appl Microbiol. Biot.* **2009**, *82*, 815 – 827.
[7] C. E. Wyman, B. E. Dale, R. T. Elander, M. Holtzapple, M. R. Ladisch, Y. Y. Lee, *Bioresour. Technol.* **2005**, *96*, 1959 – 1966.
[8] N. Mosier, C. Wyman, B. Dale, R. Elander, Y. Y. Lee, M. Holtzapple, M. Ladisch, *Bioresour. Technol.* **2005**, *96*, 673 – 686.
[9] J. Zakzeski, P. C. A. Bruijnincx, A. L. Jongerius, B. M. Weckhuysen, *Chem. Rev.* **2010**, *110*, 3552 – 3599.
[10] S. Constant, H. L. J. Wienk, A. E. Frissen, P. d. Peinder, R. Boelens, D. S. van Es, R. J. H. Grisel, B. M. Weckhuysen, W. J. J. Huijgen, R. J. A. Gosselink, P. C. A. Bruijnincx, *Green Chem.* **2016**, *18*, 2651 – 2665.
[11] S. Van den Bosch, W. Schutyser, R. Vanholme, T. Driessen, S. F. Koelewijn, T. Renders, B. De Meester, W. J. J. Huijgen, W. Dehaen, C. M. Courtin, B. Lagrain, W. Boerjan, B. F. Sels, *Energy Environ. Sci.* **2015**, *8*, 1748 – 1763.
[12] Q. Song, F. Wang, J. Cai, Y. Wang, J. Zhang, W. Yu, J. Xu, *Energy Environ. Sci.* **2013**, *6*, 994 – 1007.
[13] P. Ferrini, R. Rinaldi, *Angew. Chem. Int. Ed.* **2014**, *53*, 8634 – 8639; *Angew. Chem.* **2014**, *126*, 8778 – 8783.
[14] T. H. Parsell, B. C. Owen, I. Klein, T. M. Jarrell, C. L. Marcum, L. J. Haupert, L. M. Amundson, H. I. Kenttamaa, F. Ribeiro, J. T. Miller, M. M. Abu-Omar, *Chem. Sci.* **2013**, *4*, 806 – 813.
[15] J. M. Pepper, Y. W. Lee, *Can. J.Chemistry* **1969**, *47*, 723 – 727.
[16] E. M. Anderson, R. Katahira, M. Reed, M. G. Resch, E. M. Karp, G. T. Beckham, Y. Roman-Leshkov, *ACS Sustainable Chem. Eng.* **2016**, *4*, 6940 – 6950.
[17] M. V. Galkin, S. Sawadjoon, V. Rohde, M. Dawange, J. S. M. Samec, *ChemCatChem* **2014**, *6*, 179 – 184.
[18] P. J. Deuss, M. Scott, F. Tran, N. J. Westwood, de J. G. Vries, K. Barta, *J. Am. Chem. Soc.* **2015**, *137*, 7456 – 7467.
[19] T. Renders, S. Van den Bosch, T. Vangeel, T. Ennaert, S.-F. Koelewijn, G. Van den Bossche, C. M. Courtin, W. Schutyser, B. F. Sels, *ACS Sustainable Chem. Eng.* **2016**, *4*, 6894 – 6904.
[20] W. Schutyser, S. Van den Bosch, T. Renders, T. De Boe, S. F. Koelewijn, A. Dewaele, T. Ennaert, O. Verkinderen, B. Goderis, C. M. Courtin, B. F. Sels, *Green Chem.* **2015**, *17*, 5035 – 5045.
[21] R. M. Stephenson, *Handbook of the thermodynamics of organic compounds*. Springer Science&Business Media, Heidelberg, **2012**.
[22] A. Groysman, *Corrosion in systems for storage and transportation of petroleum products and biofuels: identification, monitoring and solutions*, Springer Science&Business Media, Heidelberg, **2014**.
[23] L. Wang, J. Zhang, X. Yi, A. Zheng, F. Deng, C. Chen, Y. Ji, F. Liu, X. Meng, F.-S. Xiao, *ACS Catal.* **2015**, *5*, 2727 – 2734.
[24] B. Güvenatam, O. Kurşun, E. H. J. Heeres, E. A. Pidko, E. J. M. Hensen, *Catal. Today* **2014**, *233*, 83 – 91.
[25] K. L. Luska, P. Migowski, El S. Sayed, W. Leitner, *Angew. Chem. Int. Ed.* **2015**, *54*, 15750 – 15755; *Angew. Chem.* **2015**, *127*, 15976 – 15981.
[26] W. Schutyser, G. Van den Bossche, A. Raaffels, S. Van den Bosch, S.-F. Koelewijn, T. Renders, B. F. Sels, *ACS Sustainable Chem. Eng.* **2016**, *4*, 5336 – 5346.
[27] P. M. Mortensen, J.-D. Grunwaldt, P. A. Jensen, A. D. Jensen, *Catal. Today* **2016**, *259*, 277 – 284.
[28] A. B. Dongil, I. T. Ghampson, R. Garcia, J. L. G. Fierro, N. Escalona, *RSC Adv.* **2016**, *6*, 2611 – 2623.
[29] T. Mochizuki, S.-Y. Chen, M. Toba, Y. Yoshimura, *Appl. Catal. B* **2014**, *146*, 237 – 243.
[30] X. Liu, L. Xu, G. Xu, W. Jia, Y. Ma, Y. Zhang, *ACS Catal.* **2016**, *6*, 7611 – 7620.
[31] G.-H. Wang, Z. Cao, D. Gu, N. Pfänder, A.-C. Swertz, B. Spliethoff, H.-J. Bongard, C. Weidenthaler, W. Schmidt, R. Rinaldi, F. Schüth, *Angew. Chem. Int. Ed.* **2016**, *55*, 8850 – 8855; *Angew. Chem.* **2016**, *128*, 8996 – 9001.
[32] T. R. Viljava, R. S. Komulainen, A. O. I. Krause, *Catal. Today* **2000**, *60*, 83 – 92.
[33] T. Nimmanwudipong, R. C. Runnebaum, D. E. Block, B. C. Gates, *Energy Fuels* **2011**, *25*, 3417 – 3427.
[34] X. Zhu, L. L. Lobban, R. G. Mallinson, D. E. Resasco, *J. Catal.* **2011**, *281*, 21 – 29.
[35] G. S. Foo, A. K. Rogers, M. M. Yung, C. Sievers, *ACS Catal.* **2016**, *6*, 1292 – 1307.
[36] X. Zhu, R. G. Mallinson, D. E. Resasco, *Appl. Catal. A* **2010**, *379*, 172 – 181.
[37] T. Prasomsri, A. T. To, S. Crossley, W. E. Alvarez, D. E. Resasco, *Appl. Catal. B* **2011**, *106*, 204 – 211.
[38] W.-S. Lee, A. Kumar, Z. Wang, A. Bhan, *ACS Catal.* **2015**, *5*, 4104 – 4114.
[39] M. M. Sullivan, A. Bhan, *ACS Catal.* **2016**, *6*, 1145 – 1152.
[40] M. M. Sullivan, J. T. Held, A. Bhan, *J. Catal.* **2015**, *326*, 82 – 91.
[41] W.-S. Lee, Z. Wang, R. J. Wu, A. Bhan, *J. Catal.* **2014**, *319*, 44 – 53.
[42] C.-J. Chen, W.-S. Lee, A. Bhan, *Appl. Catal. A* **2016**, *510*, 42 – 48.
[43] D. J. Rensel, S. Rouvimov, M. E. Gin, J. C. Hicks, *J. Catal.* **2013**, *305*, 256 – 263.
[44] T. Prasomsri, T. Nimmanwudipong, Y. Roman-Leshkov, *Energy Environ. Sci.* **2013**, *6*, 1732 – 1738.
[45] T. Prasomsri, M. Shetty, K. Murugappan, Y. Roman, *Energy Environ. Sci.* **2014**, *7*, 2660 – 2669.
[46] M. Shetty, K. Murugappan, T. Prasomsri, W. H. Green, Y. Román-Leshkov, *J. Catal.* **2015**, *331*, 86 – 97.
[47] S. M. Schimming, O. D. LaMont, M. König, A. K. Rogers, A. D. D'Amico, M. M. Yung, C. Sievers, *ChemSusChem* **2015**, *8*, 2073 – 2083.
[48] R. Neumann, in *Progress in Inorganic Chemistry, Vol 47*, John Wiley & Sons Inc., New York, **2007**, pp. 317 – 370.
[49] M. T. Pope, A. Müller, *Angew. Chem. Int. Ed. Engl.* **1991**, *30*, 34 – 48; *Angew. Chem.* **1991**, *103*, 56 – 70.
[50] J. H. Holles, C. J. Dillon, J. A. Labinger, M. E. Davis, *J. Catal.* **2003**, *218*, 42 – 53.
[51] G. A. Tsigdinos, C. J. Hallada, *Inorg. Chem.* **1968**, *7*, 437 – 441.
[52] L. A. Combs-Walker, C. L. Hill, *Inorg. Chem.* **1991**, *30*, 4016 – 4026.
[53] V. Kogan, Z. Aizenshtat, R. Neumann, *Angew. Chem. Int. Ed.* **1999**, *38*, 3331 – 3334; *Angew. Chem.* **1999**, *111*, 3551 – 3554.
[54] H. Benaissa, P. N. Davey, Y. Z. Khimyak, I. V. Kozhevnikov, *J. Catal.* **2008**, *253*, 244 – 252.
[55] H. Benaissa, P. N. Davey, E. F. Kozhevnikova, I. V. Kozhevnikov, *Appl. Catal. A* **2008**, *351*, 88 – 92.
[56] A. M. Khenkin, L. Weiner, Y. Wang, R. Neumann, *J. Am. Chem. Soc.* **2001**, *123*, 8531 – 8542.
[57] I. Efremenko, R. Neumann, *J. Am. Chem. Soc.* **2012**, *134*, 20669 – 20680.
[58] S. M. Schimming, G. S. Foo, O. D. LaMont, A. K. Rogers, M. M. Yung, A. D. D'Amico, C. Sievers, *J. Catal.* **2015**, *329*, 335 – 347.
[59] T. Kataoka, J. A. Dumesic, *J. Catal.* **1988**, *112*, 66 – 79.
[60] S. M. Kumbar, G. V. Shanbhag, F. Lefebvre, S. B. Halligudi, *J. Mol. Catal. A* **2006**, *256*, 324 – 334.
[61] M. I. Zaki, M. A. Hasan, F. A. Al-Sagheer, L. Pasupulety, *Colloids Surf. A* **2001**, *190*, 261 – 274.
[62] D. Carriazo, C. Domingo, C. Martín, V. Rives, *J. Solid State Chem.* **2008**, *181*, 2046 – 2057.
[63] B. M. Devassy, S. B. Halligudi, *J. Catal.* **2005**, *236*, 313 – 323.
[64] F. Ju, D. Van der Velde, E. Nikolla, *ACS Catal.* **2014**, *4*, 1358 – 1364.
[65] B. W. L. Southward, J. S. Vaughan, C. T. Oconnor, *J. Catal.* **1995**, *153*, 293 – 303.

Manuscript received: February 15, 2017
Accepted Article published: March 28, 2017
Final Article published: April 28, 2017

© 2017 Wiley-VCH Verlag GmbH & Co. KGaA, Weinheim